Hindawi Publishing Corporation
EURASIP Journal on Wireless Communications and Networking
Volume 2007, Article ID 25178, 11 pages
doi:10.1155/2007/25178

Research Article

Analysis of Filter-Bank-Based Methods for Fast Serial Acquisition of BOC-Modulated Signals

Elena Simona Lohan

Institute of Communications Engineering, Tampere University of Technology, P.O. Box 553, 33101 Tampere, Finland

Received 29 September 2006; Accepted 27 July 2007

Recommended by Anton Donner

Binary-offset-carrier (BOC) signals, selected for Galileo and modernized GPS systems, pose significant challenges for the code acquisition, due to the ambiguities (deep fades) which are present in the envelope of the correlation function (CF). This is different from the BPSK-modulated CDMA signals, where the main correlation lobe spans over 2-chip interval, without any ambiguities or deep fades. To deal with the ambiguities due to BOC modulation, one solution is to use lower steps of scanning the code phases (i.e., lower than the traditional step of 0.5 chips used for BPSK-modulated CDMA signals). Lowering the time-bin steps entails an increase in the number of timing hypotheses, and, thus, in the acquisition times. An alternative solution is to transform the ambiguous CF into an "unambiguous" CF, via adequate filtering of the signal. A generalized class of frequency-based unambiguous acquisition methods is proposed here, namely the filter-bank-based (FBB) approaches. The detailed theoretical analysis of FBB methods is given for serial-search single-dwell acquisition in single path static channels and a comparison is made with other ambiguous and unambiguous BOC acquisition methods existing in the literature.

1. INTRODUCTION

The modulation selected for modernized GPS and Galileo signals is BOC modulation, often denoted as BOC(m,n), with $m = f_{sc}/f_{ref}$, $n = f_c/f_{ref}$. Here, f_c is the chip rate, f_{sc} is the subcarrier rate, and $f_{ref} = 1.023$ MHz is the reference chip frequency (that of the C/A GPS signal) [1]. Alternatively, a BOC-modulated signal can also be defined via its BOC modulation order $N_{BOC} \triangleq 2f_{sc}/f_c$ [2–4]. Both sine and cosine BOC variants are possible (for a detailed description of sine and cosine BOC properties, see [3, 4]). The acquisition of BOC-modulated signals is challenged by the presence of several ambiguities in CF envelope (here, CF refers to the correlation between the received signal and the reference BOC-modulated code). That is, if the so-called ambiguous-BOC (aBOC) approach [5–7] is used (meaning that there is no bandlimiting filtering at the receiver or that this filter has a bandwidth sufficiently high to capture most energy of the incoming signal), the resultant CF envelope will exhibit some deep fades within ± 1 chip interval around the correct peak [5, 8], as it will be illustrated in Section 4. We remark that sometimes the term "ambiguities" refers to the multiple peaks within ± 1 chip interval around the correct peak; however, they are also related to the deep fades within this interval. The terminology used here refers to the deep fades of CF envelope.

The number of fades or ambiguities within 2-chip interval depends on the N_{BOC} order (e.g., for SinBOC, we have $2N_{BOC} - 2$ ambiguities around the maximum peak, while for CosBOC, we have $2N_{BOC}$ ambiguities [4]). The distance between successive ambiguities in the CF envelope sets an upper bound on the step of searching the time-bin hypotheses $(\Delta t)_{bin}$, in the sense that if the time-bin step becomes too high, the main lobe of the CF envelope might be lost during the acquisition. Typically, a step of one-half the distance between the correlation peak and its first zero value, or, equivalently, one quarter of the main lobe width is generally considered [9]. For example, acquisition time-bin steps of 0.5 chips are used for BPSK modulation (such as for C/A code of GPS), where the width of the main lobe is 2 chips, and steps of 0.1–0.2 chips are used for SinBOC(1,1) modulation, where the width of the main lobe is about 0.7 chips (such as for Galileo Open Service) [5, 10, 11].

In order to be able to increase the time-bin step (and, thus, the speed of the acquisition process), several Filter-Bank-Based (FBB) methods are proposed here, which exploit

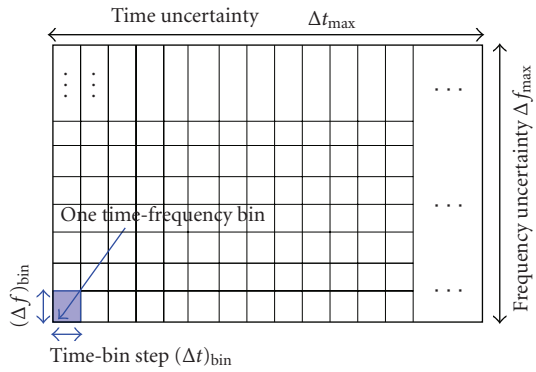

Figure 1: Illustration of the time/frequency search space.

the property that by reducing the signal bandwidth before correlation, we are able to increase the width of the CF main lobe. A thorough theoretical model is given for the characterization of the decision variable in single-path static channels and the theoretical model is validated via simulations. The proposed FBB methods are compared with two other existing methods in the literature: the classical ambiguous-BOC processing (above-mentioned) and a more recent, unambiguous-BOC technique, introduced by Fishman and Betz [9] (denoted here via B&F method, but also known as sideband correlation method or BPSK-like technique) and further analyzed and developed in [2, 6, 7, 10, 11]. It is mentioned that FBB methods have also been studied by the author in the context of hybrid-search acquisition [12]. However, the theoretical analysis of FBB methods is newly introduced here.

2. ACQUISITION PROBLEM AND AMBIGUOUS (ABOC) ACQUISITION

In Global Navigation Satellite Systems (GNSS) based on code division multiple access (CDMA), such as Galileo and GPS systems, the signal acquisition is a search process [13] which requires replication of both the code and the carrier of the space vehicle (SV) to acquire the SV signal. The range dimension is associated with the replica code and the Doppler dimension is associated with the replica carrier. Therefore, the signal match is two dimensional. The combination of one code range search increment (code bin) and one velocity search increment (Doppler bin) is a cell.

The time-frequency search space is illustrated in Figure 1. The uncertainty region represents the total number of cells (or bins) to be searched [13–15]. The cells are tested by correlating the received and locally generated codes over a dwell or integration time τ_d. The whole uncertainty region in time $\Delta t_{\max}$ is equal to the code epoch length. The length of the frequency uncertainty region $\Delta f_{\max}$ may vary according to the initial information: if assisted-GPS data are available, $\Delta f_{\max}$ can be as small as couple of Hertzs or couple of tens of Hertzs. If no Doppler-frequency information exists (i.e., no assistance or autonomous GPS), the frequency range $\Delta f_{\max}$ can be as large as few tens of kHz [13].

The time-frequency bin defines the final time-frequency error after the acquisition process and it is characterized by one correlator output: the length of a bin in time direction (or the time-bin step) is denoted by $(\Delta t)_{\text{bin}}$ (expressed in chips) and the length of a bin in frequency direction is denoted by $(\Delta f)_{\text{bin}}$. For example, for GPS case, a typical value for the $(\Delta t)_{\text{bin}}$ is 0.5 chips [13]. The search procedure can be serial (if each bin is searched serially in the uncertainty space), hybrid (if several bins are searched together), or fully parallel (if one decision variable is formed for the whole uncertainty space) [13]. This paper focuses on the serial search approach.

One of the main features of Galileo system is the introduction of longer codes than those used for most GPS signals. Also, the presence of BOC modulation creates some additional peaks in the envelope of the correlation function, as well as additional deep fades within ± 1 chip from the main peak. For this reason, a time-bin step of 0.5 chips is typically not sufficient and smaller steps need to be used [5, 10, 11]. On the other hand, decreasing the time-bin step will increase the mean acquisition time and the complexity of the receiver [9].

In the serial search code acquisition process, one decision variable is formed per each time-frequency bin (based on the correlation between the received signal and a reference code), and this decision variable is compared with a threshold in order to decide whether the signal is present or absent. The *ambiguous-BOC (aBOC) processing* means that, when forming the decision variable, the received signal is directly correlated with the reference BOC-modulated PRN sequence (all the spectrum is used for both the received signal and reference code).

3. BENCHMARK UNAMBIGUOUS ACQUISITION: B&F METHOD

The presence of BOC modulation in Galileo systems poses supplementary constraints on code search strategies, due to the ambiguities of the CF envelope. Therefore, better strategies should be used to insure reasonable performance (acquisition time and detection probabilities) as those obtained for short codes. One of the proposed strategies to deal with the ambiguities of BOC-modulated signals is the unambiguous acquisition (known under several names, such as sideband correlation method or BPSK-like technique).

The original unambiguous acquisition technique, proposed by Fishman and Betz in [9, 16], and later modified in [6, 10], uses a frequency approach, shown in Figure 2. In what follows, we denote this technique via *B&F technique*, from the initials of the main authors. The block diagrams of the B&F method (single-sideband processing) is illustrated in Figure 2, for upper sideband- (USB-) processing [9, 16]. The same is valid for the lower sideband- (LSB-) processing. The main lobe of one of the sidebands of the received signal (upper or lower) is selected via filtering and correlated with a reference code, with tentative delay $\hat{\tau}$ and reference Doppler frequency $\widehat{f_D}$. The reference code is obtained in a

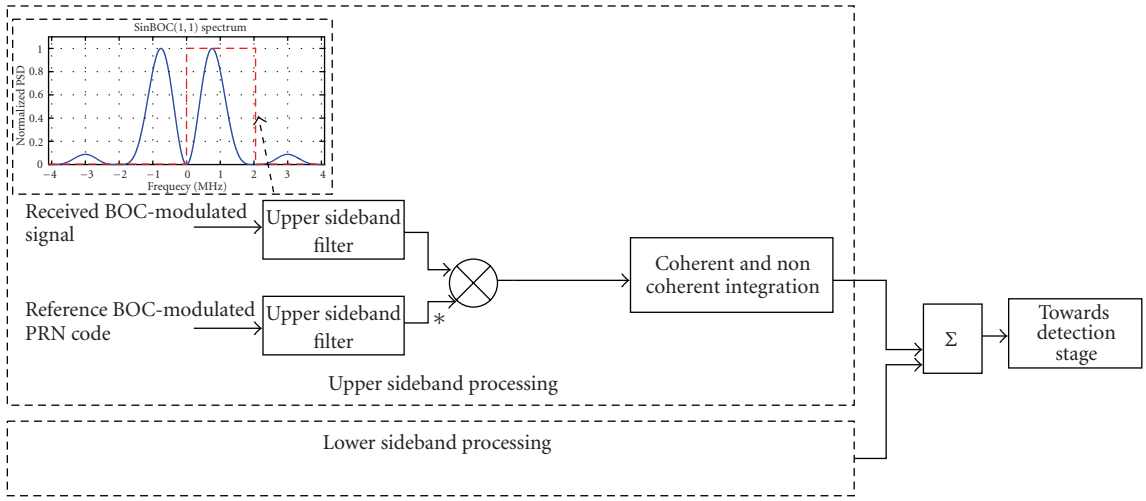

Figure 2: Block diagram of B&F method, single-sideband processing (here, upper sideband).

similar manner with the received signal, hence the autocorrelation function is no longer the CF of a BOC-modulated signal, but it will resemble the CF of a BPSK-modulated signal. However, the exact shape of the resulting CF is not identical with the CF of a BPSK-modulated signal, since some information is lost when filtering out the sidelobes adjacent to the main lobe (this is exemplified in Section 4). This filtering is needed in order to reduce the noise power. When the B&F dual-sideband method is used, we add together the USB and LSB outputs and form the dual-sideband statistic.

4. FILTER-BANK-BASED (FBB) METHODS

The underlying principle of the proposed FBB methods is illustrated in Figure 3 and the block diagram is shown in Figure 4. The number of filters in the filter bank is denoted by N_{fb} and it is related to the number of frequency pieces per sideband N_{pieces} via: $N_{\text{fb}} = 2N_{\text{pieces}}$ if dual sideband (SB) is used, or $N_{\text{fb}} = N_{\text{pieces}}$ if single SB is used. In Figure 3, the upper plot shows the spectrum of a SinBOC(1,1)-modulated signal, together with several filters (here $N_{\text{fb}} = 4$) which cover the useful part of the signal spectrum (the useful part is considered here to be everything between the main spectral lobes of the signal, including these main lobes). Alternatively, we may select only the upper (or lower) SB of the signal (i.e., single-SB processing).

The filters may have equal or unequal frequency widths. Two methods may be employed and they have been denoted here via equal-power FBB (FBB_{ep}), where each filter lets the same signal's spectral energy to be passed, thus they have unequal frequency widths (see upper plot of Figure 3), or equal-frequency-width FBB (FBB_{efw}), where all the filters in the filter bank have the same bandwidth (but the signal power is different from one band to another). An observation ought to be made here with respect to these denominations: indeed, before the correlation takes place and after filtering the incoming signal (via the filter bank), the noise power density is exactly in reverse situation compared to the signal power, since the noise power depends on the filter bandwidth (i.e., the noise power is constant from one band to another for the FBB_{efw} case, and it is variable for the FBB_{ep} case). However, the incoming (filtered) signal is correlated with the reference BOC-modulated code. Thus, the noise, which may be assumed white before the correlation, becomes coloured noise after the correlation with BOC signal, and its spectrum (after the correlation) takes the shape of the BOC power spectral density. Therefore, after the correlation stage at the receiver (e.g., immediately before the coherent integration block), both signal power density and noise power density are shaped by the BOC spectrum. Thus, the denominations used here (FBB_{ep} and FBB_{efw}) are suited for both signal and noise parts, as long as the focus is on the processing after the correlation stage (as it is the case in the acquisition).

As seen in Figure 4, the same filter bank is applied to both the signal and the reference BOC-modulated pseudorandom code. Then, filtered pieces of the signal are correlated with filtered pieces of the code (as shown in Figure 4) and an example of the resultant CF is plotted in the lower part of Figure 3. For reference purpose, also aBOC and B&F cases are shown. It is noticed that, when $N_{\text{pieces}} = 1$, the proposed FBB methods (both FBB_{ep} and FBB_{efw}) become identical with B&F method, and the higher the N_{pieces} is, the wider the main lobe of the CF envelope becomes, at the expense of a higher decrease in the signal power.

The block diagram in Figure 4 applies not only to FBB methods, but also to other GPS/Galileo acquisition methods, such as single/dual SB, and ambiguous-/unambiguous-BOC acquisition methods (i.e., aBOC corresponds to the case when no filtering stage is applied to the received and reference signals, while B&F corresponds to the case when $N_{\text{pieces}} = 1$). The complex outputs $y_i(\cdot), i = 1, \ldots, N_{\text{fb}}$ of the coherent integration block of Figure 4 can be written as

$$y_i(\hat{\tau}, \hat{f}_D, n) = \frac{1}{T_{\text{coh}}} \int_{nT}^{nT+T_{\text{coh}}} \tilde{r}_i(t) \tilde{c}_i(t - \hat{\tau}) e^{j2\pi \hat{f}_D t} dt, \quad (1)$$

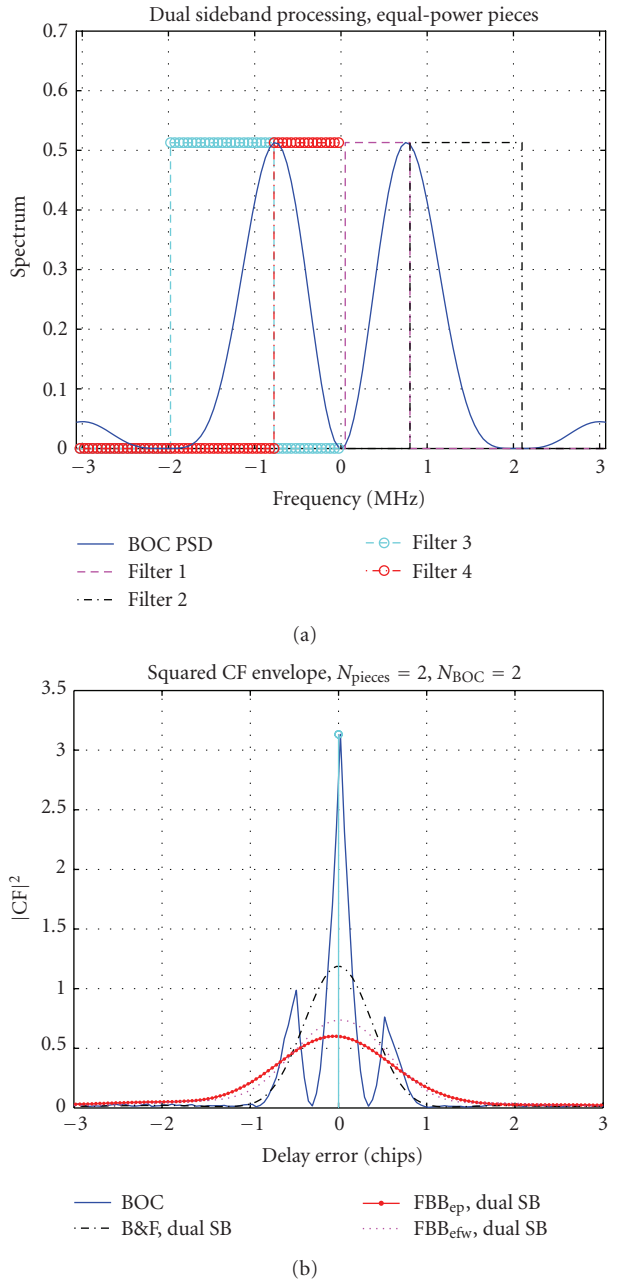

FIGURE 3: Illustration of the FBB acquisition methods, SinBOC(1,1) case. Upper plot: division into frequency pieces, via $N_{\text{fb}} = 4$ filters (FBB_{ep} method). Lower plot: squared CF shapes for 2 FBB methods, compared with ambiguous BOC (aBOC) and unambiguous Betz&Fishman (B&F) methods.

where n is the symbol (or code epoch) index, T is the symbol interval, $\widetilde{r}_i(t)$ is the filtered signal via the ith filter, $\widetilde{c}_i(t)$ is the filtered reference code (note that the code $c(t)$ before the filter bank is the BOC-modulated spread spectrum sequence), $\widehat{\tau}$ and $\widehat{f}_D$ are the receiver candidates for the delay and Doppler shift, respectively, and T_{coh} is the coherent integration length (if the code epoch length is 1 millisecond, then the number of coherent code epochs N_c may be used instead: $T_{\text{coh}} = N_c$ ms). Without loss of generality, we may assume that a pilot channel is available (such as it is the case of Galileo L1 band), thus the received signal $r(t)$ (before filtering) has the form

$$r(t) = \sqrt{E_b}c(t-\tau)e^{-j2\pi f_D t} + \eta_{\text{wb}}(t), \tag{2}$$

where τ and f_D are the delay and Doppler shift introduced by the channel, $\eta_{\text{wb}}(t)$ is the additive white Gaussian noise at wideband level, and E_b is the bit energy.

The coherent integration outputs $y_i(\cdot)$ are Gaussian processes (since a filtered Gaussian processes is still a Gaussian processes). Their mean is either 0 (if we are in an incorrect time-frequency bin) or it is proportional to a time-Doppler deterioration factor $\sqrt{E_b}\mathcal{F}(\Delta\widehat{\tau}, \Delta\widehat{f}_D)$ [11], with a proportionality constant dependent on the number of filters and of the acquisition algorithm, as it will be shown in Section 5. Here, $\mathcal{F}(\cdot)$ is the amplitude deterioration in the correct bin due to a residual time error $\Delta\widehat{\tau}$ and a residual Doppler error $\Delta\widehat{f}_D$ [11]

$$\mathcal{F}(\Delta\widehat{\tau}, \Delta\widehat{f}_D) = \left| \mathcal{R}(\Delta\widehat{\tau}) \frac{\sin(\pi\Delta\widehat{f}_D T_{\text{coh}})}{\pi\Delta\widehat{f}_D T_{\text{coh}}} \right|. \tag{3}$$

As mentioned above, $\Delta\widehat{\tau} = \tau - \widehat{\tau}$, $\Delta\widehat{f}_D = f_D - \widehat{f}_D$, and $\mathcal{R}(\Delta\widehat{\tau})$ is the CF value at delay error $\Delta\widehat{\tau}$ (CF is dependent on the used algorithm, as shown in the lower plot of Figure 3). Moreover, if we normalize the $y_i(\cdot)$ variables with respect to their maximum power, the variance of $y_i(\cdot)$ variables (in both the correct and incorrect bins) is proportional to the postintegration noise variance

$$\sigma^2 \triangleq 10^{-(\text{CNR}+10\log_{10}T_{\text{coh}})/10}, \tag{4}$$

where $\text{CNR} = E_b B_W / N_0$ is the Carrier-to-Noise Ratio, expressed in dB-Hz [5, 7, 11], B_W is the signal bandwidth after despreading (e.g., $B_W = 1$ kHz for GPS and Galileo signals), and N_0 is the double-sided noise spectral power density in the narrowband domain (after despreading or correlation on 1 millisecond in GPS/Galileo). The proportionality constants are presented in Section 5. The decision statistic Z of Figure 4 is the output of noncoherent combining of $N_{\text{nc}}N_{\text{fb}}$ complex Gaussian variables, where N_{nc} is the noncoherent integration time (expressed in blocks of N_c ms):

$$Z = \frac{1}{N_{\text{nc}}} \frac{1}{N_{\text{fb}}} \sum_{n=1}^{N_{\text{nc}}} \sum_{i=1}^{N_{\text{fb}}} |\, y_i(\widehat{\tau}, \widehat{f}_D, n)\,|^2. \tag{5}$$

We remark that the coloured noise impact on Z statistic is similar with the impact of a white noise; the only difference will be in the moments of Z, as discussed in Section 5.1 (since a filtered Gaussian variable is still a Gaussian variable, but with different mean and variance, according to the used filter). Thus, if those Gaussian variables have equal variances, Z is a chi-square distributed variable [17, 18], whose number of degrees of freedom depends on the method and the number of filters used. Next section presents the parameters of the distribution of Z for each of the analyzed methods.

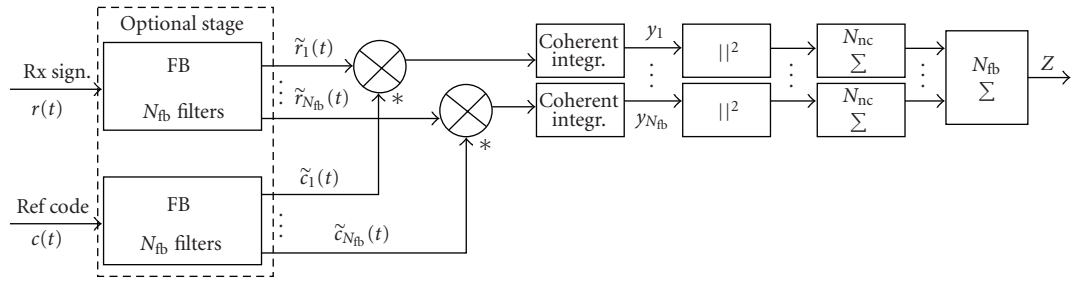

FIGURE 4: Block diagram of a generic acquisition block.

5. THEORETICAL MODEL FOR FBB ACQUISITION METHODS

5.1. Test statistic distribution

As explained above, the test statistic Z for aBOC, B&F, and proposed FBB_{ep} approaches[1] is either a central or a noncentral χ^2-distributed variable with N_{deg} degrees of freedom, according to whether we have an incorrect (bin $\triangleq \mathcal{H}_0$) or a correct (bin $\triangleq \mathcal{H}_1$) time-frequency bin, respectively. Its noncentrality parameter λ_Z and its variance σ_Z^2 are thus given by

$$\begin{aligned} \lambda_Z &= \xi_{\lambda_{\text{bin}}} \left| \mathcal{F}\left(\Delta\widehat{\tau}, \Delta\widehat{f}_D\right) \right|, \\ \sigma_Z^2 &= \xi_{\sigma^2_{\text{bin}}} \frac{\sigma^2}{N_{\text{nc}}}, \end{aligned} \tag{6}$$

where $\mathcal{F}(\cdot)$ is given in (3), σ^2 is given in (4), and $\xi_{\sigma^2_{\text{bin}}}$ and $\xi_{\lambda_{\text{bin}}}$ are two algorithm-dependent factors shown in Table 1 (they also depend on whether we are in a correct bin or in an incorrect bin). We remark that the noncentrality parameter used here is the square-root of the noncentrality parameter defined in [17], such that it corresponds to amplitude levels (and not to power levels). The relationship between the distribution functions and their noncentrality parameter and variance will be given in (8).

All the parameters in Table 1 have been derived by intuitive reasoning (explained below), followed by a thorough verification of the theoretical formulas via simulations. For clarity reasons, we assumed that the bit energy is normalized to $E_b = 1$ and all the signal and noise statistics are present with respect to this normalization.

Clearly, for aBOC algorithm, $\xi_{\sigma^2_{\text{bin}}} = 1$ and the noncentrality factor $\xi_{\lambda_{\text{bin}}}$ is either 1 (in a correct bin) or 0 (in an incorrect bin) [5, 7, 19]. Also, $N_{\text{deg}} = 2N_{\text{nc}}$ for aBOC, because we add together the absolute-squared valued of N_{nc} complex variables (or the squares $2N_{\text{nc}}$ real variables, coming from real and imaginary parts of the correlator outputs). For B&F, the noncentrality deterioration factor and the variance deterioration factor depend on the normalized power per main lobe (positive or negative) P_{ml} of the BOC power spectral density (PSD) function. P_{ml} can be easy computed analytically, using, for example, the formulas for PSD given in [3, 4] and some illustrative examples are shown in Figure 5; the normalization is done with respect to the total signal power, thus $P_{\text{ml}} < 0.5$.; P_{ml} factor is normalized with respect to the total signal power, thus $P_{\text{ml}} < 0.5$ (e.g., $P_{\text{ml}} = 0.428$ for Sin-BOC(1,1)). The decrease in the signal and noise power after the correlation in B&F method (and thus, the decrease in $\xi_{\lambda_{\mathcal{H}_1}}$ and $\xi_{\sigma^2_{\text{bin}}}$ parameters) is due to the fact that both the signal and the reference code are filtered and the filter bandwidth is adjusted to the width of the PSD main lobe. Also, in dual-SB approaches, the signal power is twice the signal power for single SB, therefore, the noncentrality parameter (which is a measure of the amplitude, not of the signal power) increases by $\sqrt{2}$. Furthermore, in dual-SB approaches, we add a double number of noncoherent variables, thus the number of degrees of freedom is doubled compared to single-SB approaches.

The derivation of χ^2 parameters for FBB_{ep} is also straightforward by keeping in mind that the variance of the variables y_i is constant for each frequency piece (the filters were designed in such a way to let equal power to be passed through them). Thus, the noise power decrease factor is $\xi_{\sigma^2_{\text{bin}}} = P_{\text{ml}}/N_{\text{pieces}}$, bin $= \mathcal{H}_0, \mathcal{H}_1$, and the signal power decreases to $N_{\text{pieces}}(P^2_{\text{ml}}/N^2_{\text{pieces}})$, thus $x_{\lambda_{\text{bin}}} = P_{\text{ml}}/\sqrt{N_{\text{pieces}}}$ for single SB (and $x_{\lambda_{\text{bin}}} = \sqrt{2}P_{\text{ml}}/\sqrt{N_{\text{pieces}}}$ for dual SB).

For FBB_{efw}, the reasoning is not so straightforward (because the sum of squares of Gaussian variables of different variances is no longer χ^2 distributed) and the bounds given in Table 1 were obtained via simulations. It was noticed (via simulations) that the noise variance in the correct and incorrect bins is no longer the same. It was also noticed that the distribution of FBB_{efw} test statistic is bounded by two χ^2 distributions. Moreover, $P_{\max_{\text{pp}}}$ is the maximum power per piece (in the positive or in the negative frequency band). For example, if $N_{\text{pieces}} = 2$ and FBB_{efw} approach is used for Sin-BOC(1,1) case, the powers per piece of the positive-sideband lobe are 0.10 and 0.34, respectively (hence, $P_{\max_{\text{pp}}} = 0.34$). Again, these powers can be derived straightforwardly, via the formulas shown in [1, 3, 4, 20].

Figure 6 compares the simulation-based complementary CDF (i.e., 1-CDF) with theoretical complementary CDFs for FBB_{ep} case (similar plots were obtained for aBOC, B&F, and FBB_{efw} but they are not included here due to

[1] The case of FBB_{efw} is discussed separately, later in this section.

Table 1: χ^2 parameters for the distribution of the decision variable Z, various acquisition methods.

	Correct bin (hypothesis $\mathcal{H}_1$)			Incorrect bin (hypothesis $\mathcal{H}_0$)		
	$\xi_{\lambda_{\mathcal{H}_1}}$	$\xi_{\sigma^2_{\mathcal{H}_1}}$	N_{deg}	$\xi_{\lambda_{\mathcal{H}_0}}$	$\xi_{\sigma^2_{\mathcal{H}_0}}$	N_{deg}
aBOC	1	1	$2N_{\text{nc}}$	0	1	$2N_{\text{nc}}$
Single-sideband B& F	P_{ml}	P_{ml}	$2N_{\text{nc}}$	0	P_{ml}	$2N_{\text{nc}}$
Dual-sideband B&F	$\sqrt{2}P_{\text{ml}}$	P_{ml}	$4N_{\text{nc}}$	0	P_{ml}	$4N_{\text{nc}}$
Single-sideband FBB_{ep} and lower bound of single-sideband FBB_{efw}	$\frac{P_{\text{ml}}}{\sqrt{N_{\text{pieces}}}}$	$\frac{P_{\text{ml}}}{N_{\text{pieces}}}$	$2N_{\text{nc}}N_{\text{pieces}}$	0	$\frac{P_{\text{ml}}}{N_{\text{pieces}}}$	$2N_{\text{nc}}N_{\text{pieces}}$
Dual-sideband FBB_{ep} and lower bound of dual-sideband FBB_{efw}	$\sqrt{2}\frac{P_{\text{ml}}}{\sqrt{N_{\text{pieces}}}}$	$\frac{P_{\text{ml}}}{N_{\text{pieces}}}$	$4N_{\text{nc}}N_{\text{pieces}}$	0	$\frac{P_{\text{ml}}}{N_{\text{pieces}}}$	$4N_{\text{nc}}N_{\text{pieces}}$
Upper bound of single-sideband FBB_{efw}	$\frac{P_{\text{ml}}}{\sqrt{N_{\text{pieces}}}}$	$\frac{P_{\text{max}_{\text{pp}}}}{N_{\text{pieces}}}$	$2N_{\text{nc}}N_{\text{pieces}}$	0	$\frac{P_{\text{ml}}}{N_{\text{pieces}}}$	$2N_{\text{nc}}N_{\text{pieces}}$
Upper bound of dual-sideband FBB_{efw}	$\sqrt{2}\frac{P_{\text{ml}}}{\sqrt{N_{\text{pieces}}}}$	$\frac{P_{\text{max}_{\text{pp}}}}{N_{\text{pieces}}}$	$4N_{\text{nc}}N_{\text{pieces}}$	0	$\frac{P_{\text{ml}}}{N_{\text{pieces}}}$	$4N_{\text{nc}}N_{\text{pieces}}$

lack of space). For the simulations shown in Figure 6, SinBOC(1,1) signal was used, with coherent integration length $N_c = 20$ milliseconds, noncoherent integration length $N_{\text{nc}} = 2$, CNR = 24 dB-Hz, number of samples per BOC interval $N_s = 4$, and single-SB filter bank with 4 filters (i.e., $N_{\text{fb}} = N_{\text{pieces}} = 4$). It was also noticed that the bounds for FBB_{efw} approach are rather loose. However, simulation results showed that the average behavior of FBB_{efw}, while keeping between the bounds, is also very similar with the average behavior of FBB_{ep} [12], therefore, from now on, it is possible to rely on FBB_{ep} curves alone in order to illustrate the average performance of proposed FBB methods. We remark that the plots of complementary CDF were chosen instead of CDF, in order to show better the tail matching of the theoretical and simulation-based distributions.

5.2. Detection probability and mean acquisition times

In serial search acquisition, the detection probability per bin $P_{d_{\text{bin}}}(\Delta\hat{\tau})$ is the probability that the decision variable Z is higher than the decision threshold γ, provided that we are in a correct bin (hypothesis $\mathcal{H}_1$). Similarly, the false alarm probability P_{fa} is the probability that the decision variable is higher than γ, provided that we are in an incorrect bin (hypothesis $\mathcal{H}_0$). These probabilities can be easily computed based on the cumulative distribution functions (CDFs) of Z in the correct $F_{\text{nc}}(\cdot)$ and incorrect bins $F_c(\cdot)$ [11]:

$$P_{d_{\text{bin}}}(\Delta\hat{\tau}, \Delta\hat{f}_D) = 1 - F_{\text{nc}}(\gamma, \lambda_Z),$$
$$P_{\text{fa}} = 1 - F_c(\gamma), \tag{7}$$

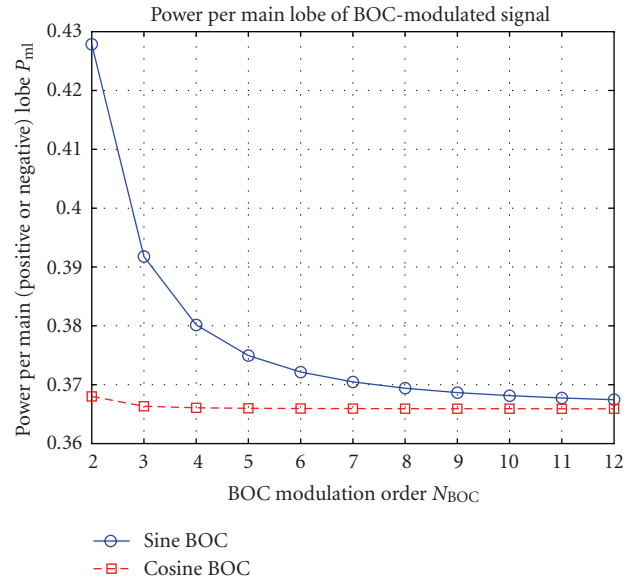

Figure 5: Normalized power per main lobe P_{ml} for BOC-modulated signals for various N_{BOC} orders.

where $F_{\text{nc}}(\cdot)$ is the CDF of a noncentral χ^2 variable and $F_c(\cdot)$ is the CDF of a central χ^2 variable, given by [17]:

$$F_c(z) = 1 - \sum_{k=0}^{N_{\text{deg}}/2-1} e^{-z/\sigma_Z^2}\left(\frac{z}{\sigma_Z^2}\right)^k \frac{1}{k!} \quad \text{in incorrect bins } \mathcal{H}_0$$
$$F_{\text{nc}}(z, \lambda_Z) = 1 - Q_{N_{\text{deg}}/2}\left(\frac{\lambda_Z\sqrt{2}}{\sigma_Z}, \frac{\sqrt{2z}}{\sigma_Z}\right) \quad \text{in correct bins } \mathcal{H}_1 \tag{8}$$

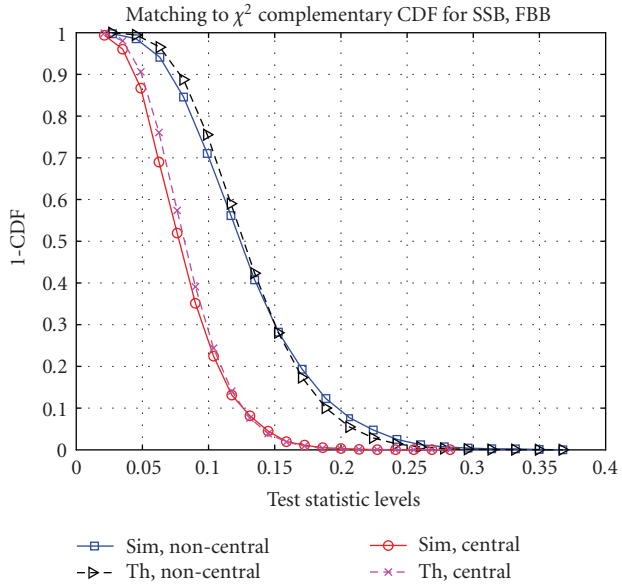

FIGURE 6: Matching with χ^2 distributions, (complementary CDF: 1-CDF), theory (th) versus simulations (sim), FBB_{ep}, $N_{\text{fb}} = N_{\text{pieces}} = 4$.

with σ_Z^2, N_{deg}, and λ_Z given in (6) and in Table 1, and $Q_{N_{\text{deg}}/2}(\cdot)$ being the generalized Marcum-Q function [17]. Due to the fact that the time-bin step may be smaller than the 2-chip interval of the CF main lobe, we might have several correct bins. The number of correct bins is: $N_t = \lfloor 2T_c/(\Delta t)_{\text{bin}} \rfloor$, where T_c is the chip interval. Thus, the global detection probability P_d is the sum of probabilities of detecting the signal in the ith bin, provided that all the previous tested hypotheses for the prior correct bins gave a misdetection [11]:

$$P_d(\Delta\tau_0) = \sum_{k=0}^{N_t-1} P_{d_{\text{bin}}}(\Delta\tau_0 + k(\Delta t)_{\text{bin}}, \Delta\hat{f}_D) \prod_{i=0}^{k-1} \left(1 - P_{d_{\text{bin}}}(\Delta\tau_0 + i(\Delta t)_{\text{bin}}, \Delta\hat{f}_D)\right). \tag{9}$$

In (9), $\Delta\tau_0$ is the delay error associated with the first sampling point in the two-chip interval, where we have N_t correct bins. Equation (9) is valid only for fixed sampling points. However, due to the random nature of the channels, the sampling point (with respect to the channel delay) is randomly fluctuating, hence, the global P_d is computed as the expectation $\text{E}(\cdot)$ over all possible initial delay errors (under uniform distribution, we simply take the temporal mean):

$$P_d = \text{E}_{\Delta\tau_0}(P_d(\Delta\tau_0)), \tag{10}$$

and the worst detection probability is obtained for the worst sequence of sampling points: $P_{d,\text{worst}} = \min_{\Delta\tau_0}(P_d(\Delta\tau_0))$.

The mean acquisition time $\overline{T}_{\text{acq}}$ for the serial search is computed according to the global P_d, the false alarm P_{fa}, the penalty time K_{penalty} (i.e., the time lost to restart the acquisition process if a false alarm state is reached), and the total number of bins in the search space [21]:

$$\overline{T}_{\text{acq}} = \frac{2 + (2 - P_d)(q-1)(1 + K_{\text{penalty}}P_{\text{fa}})}{2P_d}\tau_d, \tag{11}$$

where $\tau_d = N_{\text{nc}}T_{\text{coh}}$ is the dwell time, q is the total number of bins in the search space, and P_d and P_{fa} are given by (7) to (10). An example of the theoretical average detection probability P_d compared with the simulation results is shown in Figure 7, where a very good match is observed. The small mismatch at high $(\Delta t)_{\text{bin}}$ for the dual B&F method can be explained by the number of points used in the statistics: about 5000 random points have been used to build such statistics, which seemed enough for most of $(\Delta t)_{\text{bin}}$ ranges. However, at very low detection probabilities, this number is still too small for a perfect match. However, the gap is not significant, and low P_d regions are not the most interesting from the analysis point of view.

An example of performance (in terms of average and worst detection probabilities) of the proposed FBB methods is given in Figure 8. The gap between proposed FBB methods and aBOC method is even higher from the point of view of the worst P_d. Here, SinBOC(1,1)-modulated signal was used, and $N_c = 20$ ms, $N_{\text{nc}} = 2$. The other parameters are specified in the figures captions. The small edge in aBOC average performance at around 0.7 chips is explained by the fact that a time-bin step equal to the width of the main lobe of CF envelope (i.e., about 0.7 chips) would give worse performance than a slightly higher or smaller steps, due to ambiguities in the CF envelope. Also, the relatively constant slope in the region of 0.7–1 chips can be explained by the combination of high time-bin steps and the presence of the deep fades in the CF: since the spacing between those deep fades is around 0.7 chips for SinBOC(1,1), then a time-bin step of 0.7 chips is the worst possible choice in the interval up to 1 chip. However, there is no significant difference in average P_d for time-bin steps between 0.7 and 1 chip, since two counter-effects are superposed (and they seem to cancel each other in the region of 0.7 till 1 chip from the point of view of average P_d): on one hand, increasing the time-bin step is deteriorating the performance; on the other hand, avoiding (as much as possible) the deep fades of CF is beneficial. This fact is even more visible from the lower plot of Figure 8, where worst-case P_d are shown. Clearly, having a time-bin step of about 0.7 chips would mean that, in the worst case, we are always in a deep fade and lose completely the peak of the main lobe. This explains the minimum P_d achieved at such a step. Also, for steps higher than 1.5 chips, there is always a sampling sequence that will miss completely the main lobe of the envelope of CF (thus, the worst P_d will be zero).

It is noticed that FBB methods can work with time-bin steps higher than 1 chip, due to the increase in the main lobe of the CF envelope. Moreover, the proposed FBB methods (both single and dual SB) outperform the B&F and aBOC method if the step $(\Delta t)_{\text{bin}}$ is sufficiently high. Indeed, the higher the time-bin step, the higher is the improvement of FBB methods over aBOC and B&F methods. We remark that even at $(\Delta t)_{\text{bin}} = 1$ chip, we have a significantly high P_d,

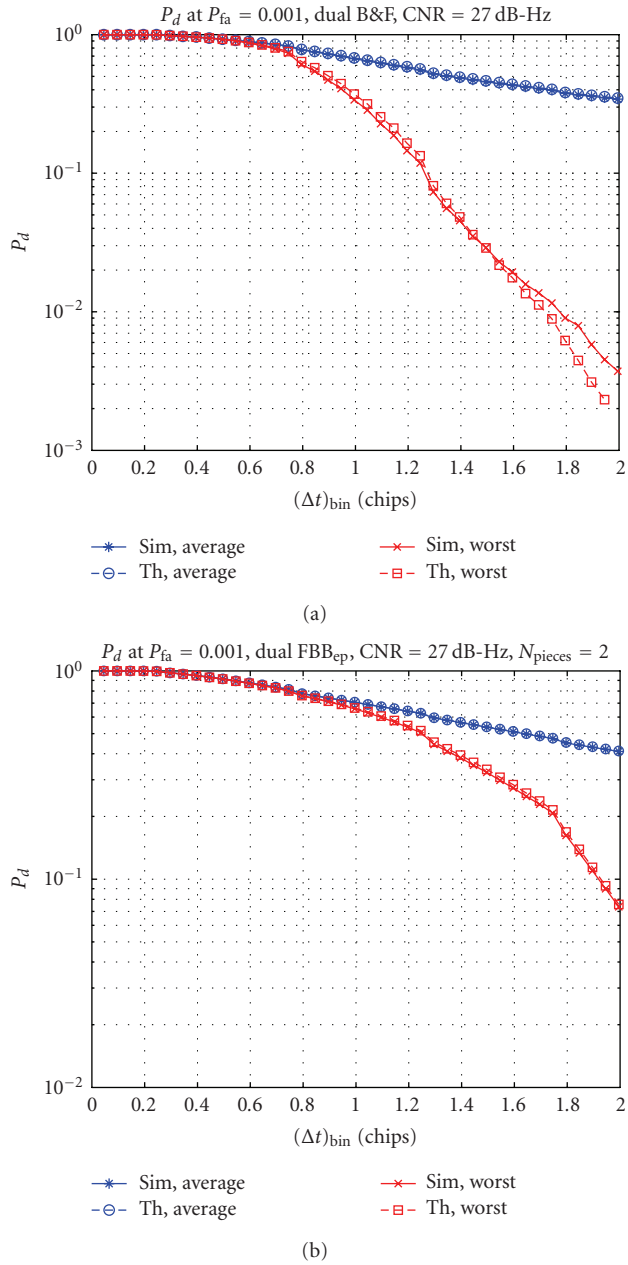

Figure 7: Comparison between theory and simulations for Sin-BOC(1,1). Left: dual-sideband B&F method. Right: Dual-sideband FBB$_{ep}$ method, $N_{pieces} = 2$. $N_c = 10$ milliseconds, $N_{nc} = 5$, CNR = 27 dB-Hz, $N_s = 5$.

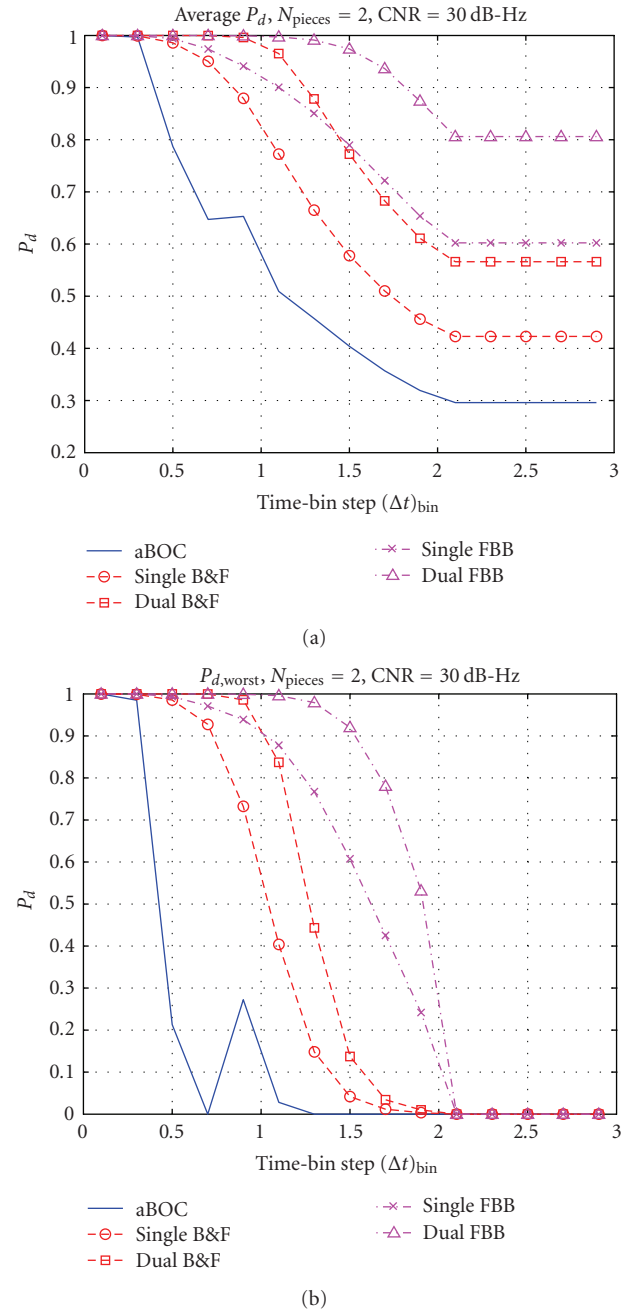

Figure 8: Average (upper) and worst (lower) detection probabilities versus $(\Delta t)_{bin}$ ambiguous and unambiguous BOC acquisition methods (FBB$_{ep}$ was used here).

due to the widening of the CF main lobe. The constant P_d at higher time-bin steps is explained by the fact that, if the step increases with respect to the correlation function width, only noise is captured in the acquisition block. Thus, increasing the step above a certain threshold would not change the serial detection probability, since the decision variable will only contains noise samples.

On the other hand, by increasing the time-bin step in the acquisition process, we may decrease substantially the mean acquisition time, because the number of bins in the search space (see (11) is directly proportional to $(\Delta t)_{bin}$. For example, if the code epoch length is 1023 chips and only one frequency bin is searched (assisted acquisition), $q = \lceil 1023/(\Delta t)_{bin} \rceil$. Moreover, the computational load required for implementing a correlator acquisition receiver per unit of time uncertainty is inversely proportional to $(\Delta t)^2_{bin}$ [9], thus, when $(\Delta t)_{bin}$ increases, the computational load decreases.

An example regarding the needed time-bin step in order to achieve a certain detection probability, at fixed CNR and false alarm probability, is shown in what follows. We

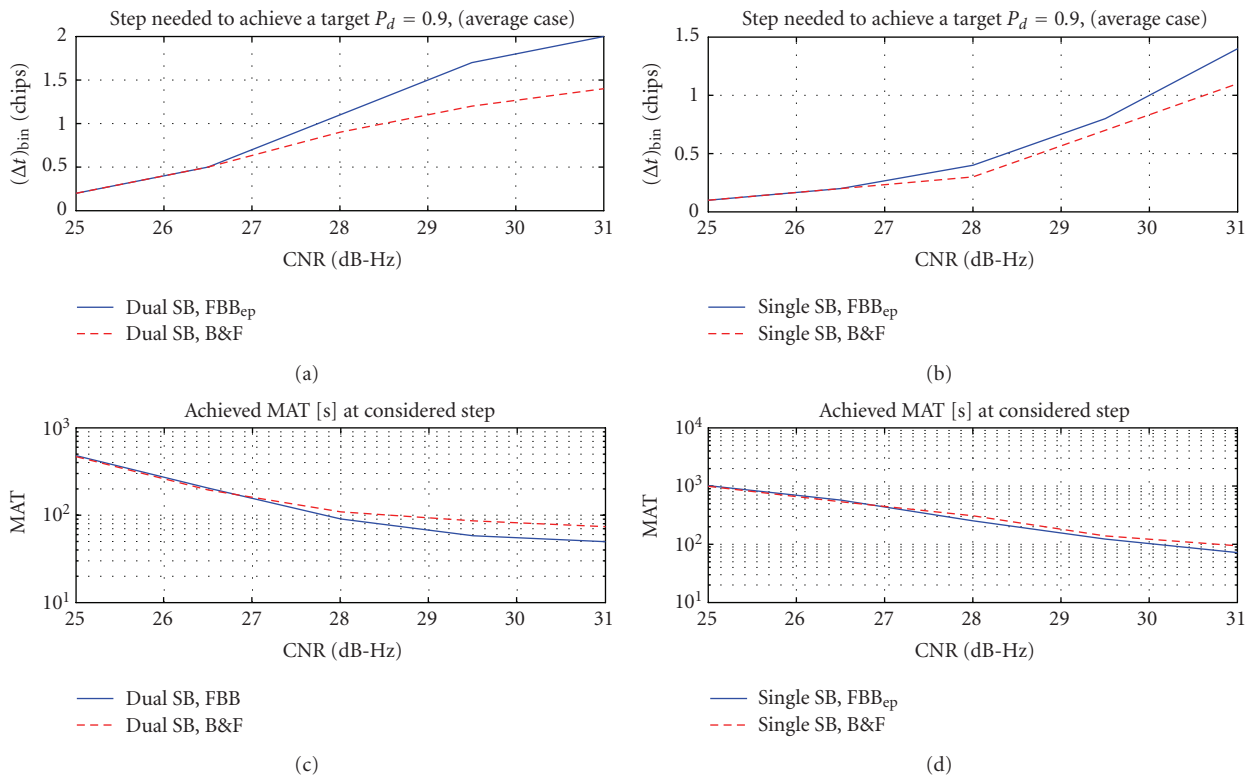

FIGURE 9: Step needed to achieve a target average $P_d = 0.9$, at false alarm $P_{\text{fa}} = 10^{-3}$ and corresponding mean acquisition time, SinBOC(1,1) signal. Code length 4092 chips, penalty factor $K_{\text{penalty}} = 1$, single frequency-bin. $N_{\text{pieces}} = 2$ for FBB$_{\text{ep}}$. Left: dual sideband. Right: single sideband.

assume a SinBOC(1,1)-modulated signal, a CNR = 30 dB-Hz, and a target average detection probability of $P_d = 0.9$ at $P_{\text{fa}} = 10^{-3}$. For these values, we need a step of $(\Delta t)_{\text{bin}} = 1.2$ chips for the dual-sideband B&F method (which will correspond to a mean acquisition time $\overline{T}_{\text{acq}} = 86.24$ s for single frequency serial search and 4092-chip length code) and a step of $(\Delta t)_{\text{bin}} = 1.7$ chips for dual-sideband FBB$_{\text{ep}}$ method with $N_{\text{pieces}} = 2$ (i.e., $\overline{T}_{\text{acq}} = 58.14$ s). Thus, the step can be about 50% higher for dual-sideband FBB case than for dual-sideband B&F case, and we may gain about 48% in the MAT (i.e., MAT is 48% less in dual-SB FBB case than in dual-SB B&F case). For single-sideband approaches, the differences between FBB and B&F methods are smaller. An illustrative plots is shown in Figure 9, where the needed steps and the achievable mean acquisition times are given with respect to CNR. We notice that FBB methods outperform B&F methods at high CNRs. Below a certain CNR limit (which, of course, depends on the $(N_c,\ N_{\text{nc}})$ pair), B&F method may be better than FBB method.

The optimal number of pieces or filters to be used in the filter bank depends on the CNR, on the method (single or dual SB), and on the BOC modulation orders. From simulation results (not included here due to lack of space), best values between 2 and 6 have been observed. This is due to the fact that a too high N_{pieces} parameter would deteriorate the signal power too much.

We remark that the choice of the penalty factor has not been documented well in the literature. The penalty time selection is in general related to the quality of the following code tracking circuit. There is a wide range of values that K_{penalty} may take and no general rule about the choice of K_{penalty} has been given so far, to the author's knowledge. For example, in [22] a penalty factor $K_{\text{penalty}} = 1$ was considered; in [23] simulations were carried out for $K_{\text{penalty}} = 2$, in [24] a penalty factor of $K_{\text{penalty}} = 10^3$ was used, while in [25] we have $K_{\text{penalty}} = 10^6$. Penalty factors with respect to dwell times were also used in the literature, for example: $K_{\text{penalty}} = 10^5/(N_cN_{\text{nc}})$ [26, 27], or $K_{\text{penalty}} = 10^7/(N_cN_{\text{nc}})$ [27] (in our simulations, $N_cN_{\text{nc}} = 40$ ms). Therefore, K_{penalty} may spread over an interval of $[1,\ 10^6]$, therefore, in our simulations we considered the 2 extreme cases: $K_{\text{penalty}} = 1$ (Figure 9) and $K_{\text{penalty}} = 10^6$ (Figure 10). Figure 10 uses exactly the same parameters as Figure 9, with the exception of the penalty factor, which is now $K_{\text{penalty}} = 10^6$. For $K_{\text{penalty}} = 10^6$ of Figure 10, MAT for the dual-sideband B&F method becomes $\overline{T}_{\text{acq}} = 8.62 * 10^4$, which is still higher than MAT for the dual-sideband FBB$_{\text{ep}}$ ($\overline{T}_{\text{acq}} = 5.8 * 10^4$ s). Similar improvements in MAT times via FBB processing (as for $K_{\text{penalty}} = 1$) are observed if we increase the penalty time.

The plots with respect to the receiver operating characteristics (ROC) are shown in Figure 11 for a CNR of 30 dB-Hz. ROC curves are obtained by plotting the misdetection probability $1 - P_d$ versus false alarm probability P_{fa} [28]. The lower the area below the ROC curves is, the better the performance of the algorithm is. As seen in Figure 11, the dual sideband unambiguous methods have the best performance.

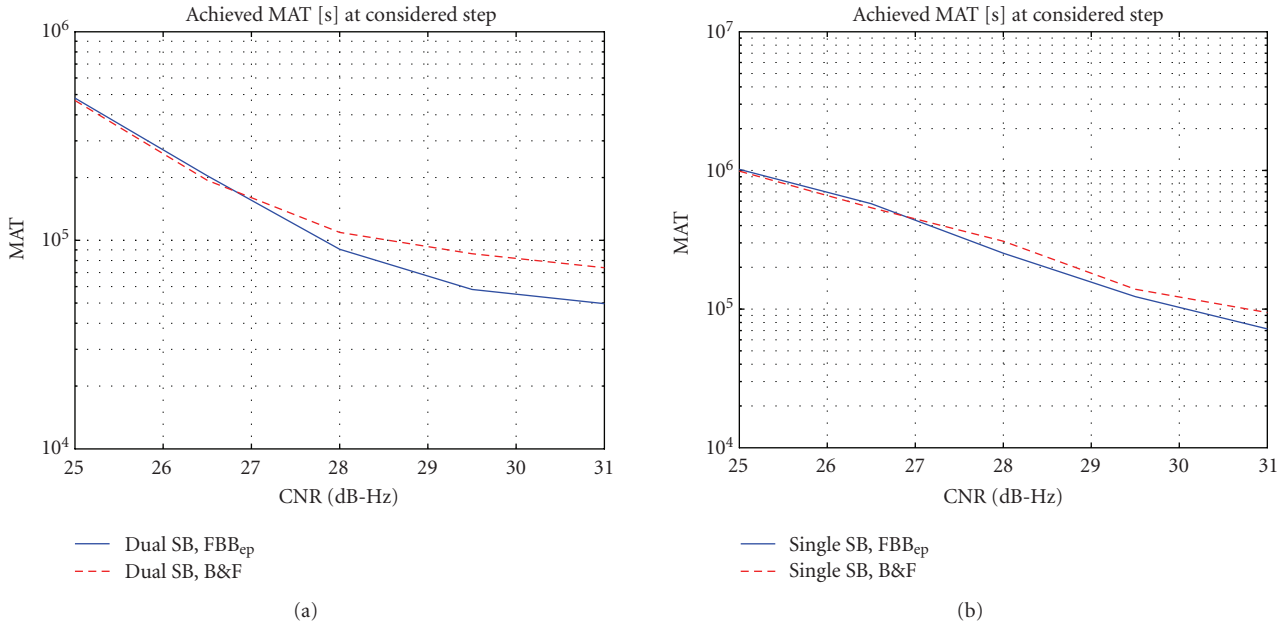

FIGURE 10: Mean acquisition time corresponding to the step needed to achieve a target average $P_d = 0.9$, at false alarm $P_{fa} = 10^{-3}$, SinBOC(1,1) signal. Code length 4092 chips, penalty factor $K_{penalty} = 10^6$, single frequency-bin. $N_{pieces} = 2$ for FBB$_{ep}$. Left: dual sideband. Right: single sideband.

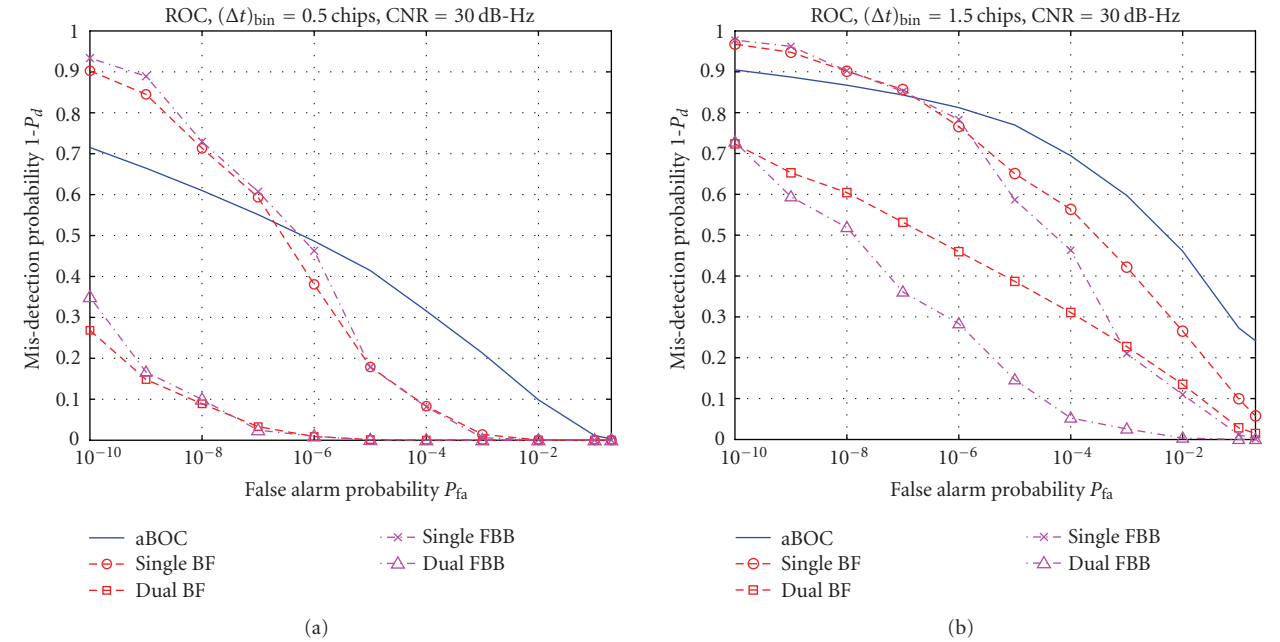

FIGURE 11: Receiver operating characteristic for CNR = 30 dB-Hz, SinBOC(1,1) signal, $N_c = 20$, $N_{nc} = 2$. Left: $(\Delta t)_{bin} = 0.5$ chips; right $(\Delta t)_{bin} = 1.5$ chips.

At low time-bin steps (e.g., $(\Delta t)_{bin} = 0.5$ chips), the FBB and B&F methods behave similarly, as it has been seen before also in Figure 8. The main advantage of FBB methods is observed for time-bin steps higher than one chip, as shown in the left plot of Figure 11. For both time-bin steps considered here, the single sideband unambiguous methods have a threshold false alarm, below which their performance becomes worse than that of ambiguous BOC approach. This threshold depends on the CNR, on the integration times, and on the time-bin step and it is typically quite low (below 10^{-5}).

6. CONCLUSIONS

This paper introduces a new class of code acquisition methods for BOC-modulated CDMA signals, based on filter bank processing. The detailed theoretical characterization of this

new method has been given and theoretical curves were validated via simulations. The performance comparison with other methods (i.e., ambiguous BOC and Betz&Fishman sideband correlator) showed that FBB techniques can be successfully employed if the target is to increase the time-bin step of the acquisition process and to minimize the mean acquisition times and the computational load of the correlator.

ACKNOWLEDGMENTS

This work was carried out in the project "Advanced Techniques for Personal Navigation (ATENA)" funded by the Finnish Funding Agency for Technology and Innovation (Tekes). This work has also been supported by the Academy of Finland.

REFERENCES

[1] J. W. Betz, "The offset carrier modulation for GPS modernization," in *Proceedings of the International Technical Meeting of the Institute of Navigation (ION-NTM '99)*, pp. 639–648, San Diego, Calif, USA, January 1999.

[2] A. Burian, E. S. Lohan, and M. Renfors, "BPSK-like methods for hybrid-search acquisition of Galileo signals," in *Proceedings of the IEEE International Conference on Communications (ICC '06)*, vol. 11, pp. 5211–5216, Istanbul, Turkey, June 2006.

[3] E. S. Lohan, A. Lakhzouri, and M. Renfors, "Binary-offset-carrier modulation techniques with applications in satellite navigation systems," *Wireless Communications and Mobile Computing*, vol. 7, no. 6, pp. 767–779, 2006.

[4] E. S. Lohan, A. Lakhzouri, and M. Renfors, "Spectral shaping of Galileo signals in the presence of frequency offsets and multipath channels," in *Proceedings of 14th IST Mobile & Wireless Communications Summit*, Dresden, Germany, June 2005, CDROM.

[5] S. Fischer, A. Guérin, and S. Berberich, "Acquisition concepts for Galileo BOC(2,2) signals in consideration of hardware limitations," in *Proceedings of the 59th IEEE Vehicular Technology Conference (VTC '04)*, vol. 5, pp. 2852–2856, Milan, Italy, May 2004.

[6] N. Martin, V. Leblond, G. Guillotel, and V. Heiries, "BOC(x,y) signal acquisition techniques and performances," in *Proceedings of the 16th International Technical Meeting of the Satellite Division of the Institute of Navigation (ION GPS/GNSS '03)*, pp. 188–198, Portland, Ore, USA, September 2003.

[7] B. Bandemer, H. Denks, A. Hornbostel, A. Konovaltsev, and P. R. Coutinho, "Performance of acquisition methods for Galileo SW receivers," in *Proceedings of the European Navigation Conference (ENC-GNSS '05)*, Munich, Germany, July 2005, CDROM.

[8] B. C. Barker, J. W. Betz, J. E. Clark, et al., "Overview of the GPS M code signal," in *Proceedings of the International Technical Meeting of the Institute of Navigation (ION-NTM '00)*, Anaheim, Calif, USA, January 2000, CDROM.

[9] P. Fishman and J. W. Betz, "Predicting performance of direct acquisition for the M-code signal," in *Proceedings of the International Technical Meeting of the Institute of Navigation (ION-NTM '00)*, pp. 574–582, Anaheim, Calif, USA, January 2000.

[10] V. Heiries, D. Roviras, L. Ries, and V. Calmettes, "Analysis of non ambiguous BOC signal acquisition performance," in *Proceedings of the 18th International Technical Meeting of the Satellite Division of the Institute of Navigation (ION-GNSS '05)*, Long Beach, Calif, USA, September 2005, CDROM.

[11] E. S. Lohan, "Statistical analysis of BPSK-like techniques for the acquisition of Galileo signals," in *Proceedings of the 23rd AIAA International Communication Systems Conference (ICSSC '05)*, Rome, Italy, September 2005, CDROM.

[12] E. S. Lohan, "Filter-bank based technique for fast acquisition of Galileo and GPS signals," in *Proceedings of the 17th IEEE International Symposium on Personal, Indoor and Mobile Radio Communications (PIMRC '06)*, pp. 1–5, Helsinki, Finland, September 2006.

[13] E. D. Kaplan, *Understanding GPS: Principles and Applications*, Artech House, London, UK, 1996.

[14] P. W. Ward, "GPS receiver search techniques," in *Proceedings of the IEEE Position Location and Navigation Symposium*, pp. 604–611, Atlanta, Ga, USA, April 1996.

[15] M. Katz, *Code acquisition in advanced CDMA networks*, Ph.D. thesis, University of Oulu, Oulu, Finland, 2002.

[16] J. Betz and P. Capozza, "System for direct acquisition of received signals," US patent no. 2004/0071200 A1, April 2004.

[17] J. Proakis, *Digital Communications*, McGraw-Hill, New York, NY, USA, 4th edition, 2001.

[18] R. R. Rick and L. B. Milstein, "Optimal decision strategies for acquisition of spread-spectrum signals in frequency-selective fading channels," *IEEE Transactions on Communications*, vol. 46, no. 5, pp. 686–694, 1998.

[19] F. Bastide, O. Julien, C. Macabiau, and B. Roturier, "Analysis of L5/E5 acquisition, tracking and data demodulation thresholds," in *Proceedings of the International Technical Meeting of the Satellite Division of the Institute of Navigation (ION-GPS '02)*, pp. 2196–2207, Portland, Ore, USA, September 2002.

[20] S. H. Raghavan and J. K. Holmes, "Modeling and simulation of mixed modulation formats for improved CDMA bandwidth efficiency," in *Proceedings of the 60th IEEE Vehicular Technology Conference (VTC '04)*, vol. 6, pp. 4290–4295, Los Angeles, Calif, USA, September 2004.

[21] J. Holmes and C. Chen, "Acquisition time performance of PN spread-spectrum systems," *IEEE Transactions on Communications*, vol. 25, no. 8, pp. 778–784, 1977.

[22] G. J. R. Povey, "Spread spectrum PN code acquisition using hybrid correlator architectures," *Wireless Personal Communications*, vol. 8, no. 2, pp. 151–164, 1998.

[23] W. Zhuang, "Noncoherent hybrid parallel PN code acquisition for CDMA mobile communications," *IEEE Transactions on Vehicular Technology*, vol. 45, no. 4, pp. 643–656, 1996.

[24] E. A. Homier and R. A. Scholtz, "Hybrid fixed-dwell-time search techniques for rapid acquisition of ultra-wideband signals," in *Proceedings of the International Workshop on Ultra-Wideband Systems*, Oulu, Finland, June 2003.

[25] B.-J. Kang and I.-K. Lee, "A performance comparison of code acquisition techniques in DS-CDMA system," *Wireless Personal Communications*, vol. 25, no. 2, pp. 163–176, 2003.

[26] O.-S. Shin and K. B. Lee, "Utilization of multipaths for spread-spectrum code acquisition in frequency-selective Rayleigh fading channels," *IEEE Transactions on Communications*, vol. 49, no. 4, pp. 734–743, 2001.

[27] D. DiCarlo and C. Weber, "Multiple dwell serial search: performance and application to direct sequence code acquisition," *IEEE Transactions on Communications*, vol. 31, no. 5, pp. 650–659, 1983.

[28] S. Soliman, S. Glazko, and P. Agashe, "GPS receiver sensitivity enhancement in wireless applications," in *Proceedings of the IEEE MTT-S International Tipical Symposium on Technologies for Wireless Applications*, pp. 181–186, Vancouver, Canada, February 1999.